ICES Journal of Marine Science Advance Access published June 14, 2015

ICES Journal of Marine Science

ICES International Council for the Exploration of the Sea
CIEM Conseil International pour l'Exploration de la Mer

ICES Journal of Marine Science; doi:10.1093/icesjms/fsv069

Characterization of distinct bloom phenology regimes in the Southern Ocean

Jean-Baptiste Sallée[1,2]*, J. Llort[1], A. Tagliabue[3], and M. Lévy[1]

[1]*Sorbonne Universités (UPMC Univ.), UMR 7159, LOCEAN-IPSL Institute, F-75005 Paris, France*
[2]*British Antarctic Survey, High Cross, Madingley Road, Cambridge CB30ET, UK*
[3]*Department of Earth, Ocean and Ecological Sciences, School of Environmental Sciences, University of Liverpool, Liverpool, UK*

**Corresponding author: e-mail: jbsallee@gmail.com*

Sallée, J-B., Llort, J., Tagliabue, A., and Lévy, M. Characterization of distinct bloom phenology regimes in the Southern Ocean. – ICES Journal of Marine Science, doi: 10.1093/icesjms/fsv069.

Received 17 September 2014; accepted 31 March 2015.

In this study, we document the regional variations of bloom phenology in the Southern Ocean, based on a 13-year product of ocean colour measurements co-located with observation-based estimates of the mixed-layer depth. One key aspect of our work is to discriminate between mixed-layer integrated blooms and surface blooms. By segregating blooms that occur before or after the winter solstice and blooms where integrated and surface biomass increase together or display a lag, we define three dominating Southern Ocean bloom regimes. While the regime definitions are solely based on bloom timing characteristics, the three regimes organize coherently in geographical space, and are associated with distinct dynamical regions of the Southern Ocean: the subtropics, the subantarctic, and the Antarctic Circumpolar Current region. All regimes have their mixed-layer integrated onset between autumn and winter, when the daylength is short and the mixed layer actively mixes and deepens. We discuss how these autumn–winter bloom onsets are controlled by either nutrient entrainment and/or reduction in prey-grazer encounter rate. In addition to the autumn–winter biomass increase, the subantarctic regime has a significant spring biomass growth associated with the shutdown of turbulence when air–sea heat flux switches from surface cooling to surface warming.

Keywords: bloom, chlorophyll, seasonal cycle, Southern Ocean.

Introduction

Satellite observations and studies based on *in situ* observations have shown that phytoplankton distribution in the Southern Ocean displays patchy regional variability (Figure 1a) and a wide range of distinct seasonal cycle regimes (e.g. Moore and Abbott, 2002; Arrigo *et al.*, 2008; Thomalla *et al.*, 2011; Chiswell *et al.*, 2013; Frants *et al.*, 2013; Carranza and Gille, 2015). While phytoplankton biomass and the associated primary productivity fluctuate according to season (e.g. Arrigo *et al.*, 2008) and location, the environmental conditions that drive these patterns are poorly understood. This hampers our ability to constrain how seasonality might be modified in the future (e.g. Henson *et al.*, 2013) and the associated implications for Southern Ocean foodwebs and biogeochemical cycling.

A unique aspect of the Southern Ocean circulation is the presence of a strong eastward, circumpolar current, the Antarctic Circumpolar Current (ACC). On the northern edge of the ACC, subtropical gyres flow anticlockwise, and their intense and energetic western boundary currents join the northern branches of the ACC in the western Atlantic, Indian, and Pacific basins. The ACC and the western boundary currents have a profound influence on the physical and biogeochemical characteristics of the Southern Ocean (Rintoul *et al.*, 2001). They form meridional dynamical barriers (Sallée *et al.*, 2008), which split the Southern Ocean into a number of distinct zones. Four main zones can be described, from north to south: the subtropical region, around 30°S, characterized by stratified surface layers (Figure 1c), and relatively weak wind and buoyancy forcing; the subantarctic region, directly north of the ACC, which is characterized by very deep mixed layers (Figure 1c), intense winds, large buoyancy forcing, and the presence of the energetic western boundary currents; the ACC region, characterized by the top-to-bottom and large circumpolar

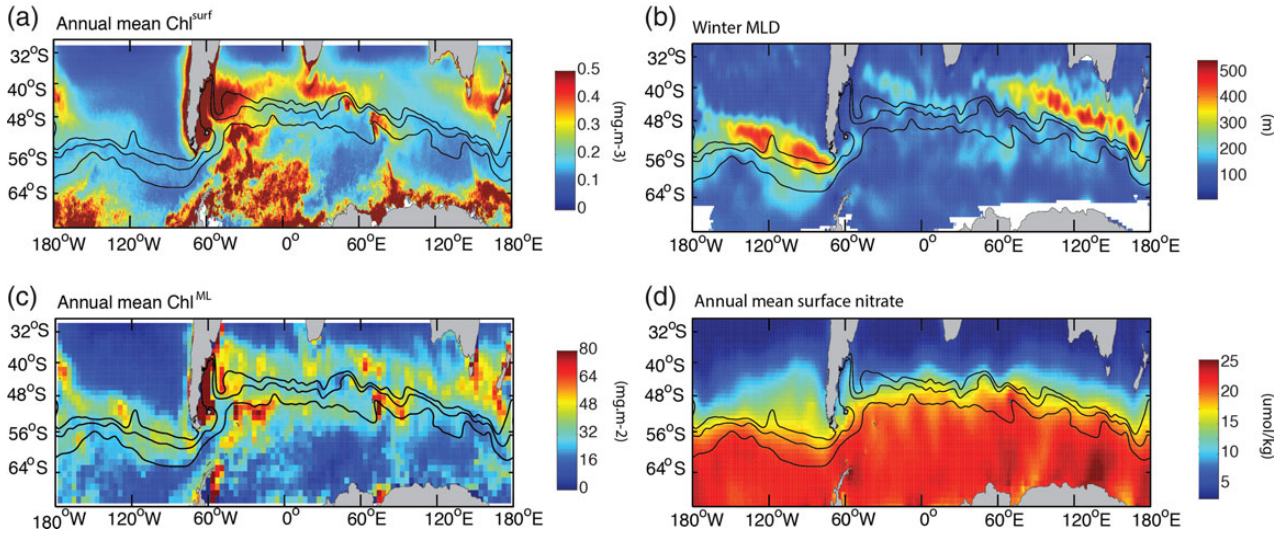

Figure 1. Climatological (a) annual mean of surface chlorophyll (Chl^{surf}; mg m^{-3}); (b) winter (September) MLD from estimated from the observational dataset; (c) annual mean mixed-layer integrated chlorophyll (Chl^{ML}; mg m^{-2}); and (d) annual mean surface nutrient concentration (μmol kg^{-1}) from the World Ocean Atlas 2009. In (a – d), the three black lines represent the approximate climatological position of the three main ACC branches, from south to north: Polar Front, subantarctic front, and northern branch of the subantarctic front following Sallée *et al.* (2008).

current; and the subpolar region, south of the ACC, characterized by the seasonal presence of sea ice, and a relatively stratified surface layer.

These dynamical zones of the Southern Ocean correspond to specific biogeochemical regions (e.g. Longhurst *et al.*, 1995). The surface layers of the subtropical region have low macronutrient concentrations (Figure 1d), the subantarctic, ACC, and subpolar regions are generally considered as macronutrient rich, iron-limited regions (e.g. Martin *et al.*, 1990; Boyd, 2002), although silicic acid is notably much lower in the subantarctic region than the ACC (e.g. Sarmiento *et al.*, 2004). Another notable aspect of the subantarctic zone is that it contains many continental sources of iron (Boyd and Ellwood, 2010), with the presence of continental plateau and many subantarctic islands, in the lee of the western boundary currents flowing eastward.

At present, it is not clear how the specific dynamical and biogeochemical regions of the Southern Ocean relate to the patchy phytoplankton distribution in the Southern Ocean (Figure 1; e.g. Thomalla *et al.*, 2011; Chiswell *et al.*, 2013).

The aim of this study is to use a range of physical and biochemical observational products to document the general chlorophyll bloom patterns in the Southern Ocean, and link these patterns to the distinct dynamical and biogeochemical regions of the Southern Ocean. Our aim of describing regional variability of the Southern Ocean phytoplankton seasonal cycle falls within the more general context of the mechanisms associated with the onset and duration of phytoplankton blooms. These mechanisms remain much debated despite decades of research (e.g. Sverdrup, 1953; Ryther and Hulburt, 1960; Evans and Parslow, 1985; Townsend *et al.*, 1992; Huisman *et al.*, 1999; Behrenfeld, 2010; Taylor and Ferrari, 2011a, b; Mahadevan *et al.*, 2012; Ferrari *et al.*, 2014). This debate arises from the wide diversity, and often inter-related, factors that control phytoplankton blooms, which range from physical (e.g. solar irradiance and the intensity of surface layer mixing), biological (e.g. growth or grazing rates), to chemical (e.g. availability or cycling of nutrients) factors.

The founding conceptual model of bloom dynamics, which arose in the first half of the last century, is the "critical depth" theory (Gran and Braarud, 1935; Riley, 1946; Sverdrup, 1953), which proposes that blooms should commence when the ocean surface mixed-layer restratifies in spring. Recently, the extent to which the mixed-layer depth (MLD) shallowing explains phytoplankton blooms has been questioned (e.g. Behrenfeld, 2010; Taylor and Ferrari, 2011a, b; Chiswell *et al.*, 2013). For instance, several authors have proposed that surface layer turbulence (primarily driven by wind and air–sea buoyancy flux) is one of the key factors for bloom onset (e.g. Huisman *et al.*, 1999; Taylor and Ferrari, 2011a, b; Chiswell *et al.*, 2013). Other works have proposed that blooms do not occur in spring, but instead in autumn or early winter, which seems to invalidate the basis of the critical depth theory (Behrenfeld, 2010; Boss and Behrenfeld, 2010). Instead, a new framework, the "disturbance-recoupling" hypothesis, has been proposed, which focuses on the balance between phytoplankton growth and grazing (Behrenfeld, 2010). Finally, some of the confusion in our understanding of phytoplankton blooms might arise from whether blooms are examined from the standpoint of water-column integrated biomass, or from surface observations (Llort *et al.*, this issue).

After presenting the datasets and methods in the Material and methods section, we introduce examples of chlorophyll seasonal cycle in the Southern Ocean. An important point in our study is that we seek to discriminate between water-column integrated chlorophyll and surface chlorophyll by co-locating surface chlorophyll observations with physical observations of the water column. One necessary assumption here is that chlorophyll is well mixed in the mixed layer and that subsurface chlorophyll are relatively uncommon or small compared with mixed-layer imprint. We demonstrate that Southern Ocean blooms can be grouped

into a number of distinct regimes based on their phenology. We then discuss the seasonal cycle of each of these regimes, before finishing with a discussion of our results.

Material and methods

Surface ocean colour product

Surface chlorophyll (Chl^{surf}) over the Southern Ocean is investigated in this study. We define the Southern Ocean as the region between the latitude 70 and 30°S. Although remote sensing of Southern Ocean chlorophyll concentrations is effective in detecting large-scale chlorophyll bloom regime, the current algorithms for the Sea-viewing Wide Field-of-view Sensor (SeaWiFS, algorithm OC4v6), the Moderate Resolution Imaging Spectroradiometer (MODIS-Aqua, algorithm OC3M), and GlobColour significantly underestimate chlorophyll concentrations at high latitudes (Johnson *et al.*, 2013). Therefore, in this study, we use a new algorithm, specifically designed for the Southern Ocean that more accurately matches long-term *in situ* datasets (Johnson *et al.*, 2013). The new algorithm improves *in situ* vs. satellite chlorophyll coefficients of determination (R2) from 0.27 to 0.46, 0.26 to 0.51, and 0.25 to 0.27, for OC4v6, OC3M, and GlobColour, respectively, while also addressing the underestimation problem. We also compared our results with the Globcolour dataset and found the definition of the regimes and their characteristics to be very similar, giving us confidence in the broad reliability of our results. However, the absolute magnitudes of blooms are affected, and as the Johnson *et al.* (2013) algorithm best matches observations, we decided to present results using this algorithm. Overall, surface chlorophyll concentrations are available at a weekly resolution, at 9 km resolution, between the years 1998 and 2010, when cloud coverage allows.

Ocean interior

To investigate the role of ocean physics in driving phytoplankton blooms, we co-located ocean temperature and salinity observations with the satellite-derived estimates of Chl^{surf}. To do this, we utilize two different ocean interior datasets, as described below.

First, defined as the "observational dataset", we use *in situ* observations of temperature/salinity profiles from a combination of the Argo float database and the ship-based Southern Ocean Data Base (SODB; see http://woceSOatlas.tamu.edu for more information). The Argo project contributes about half of the Southern Ocean profiles, fills the centre of ocean basins, and provides complete sampling over the austral winter (Sallée *et al.*, 2010). We use only profiles that have passed the Argo real-time quality control, containing information on their position, date, pressure, temperature (T), and salinity (S). Most Argo profiles sample T and S from the surface to 2000 m depth every 10 days. From this database, we extract information regarding the MLD. The advantage of this approach is that it provides ocean observations at the time and location of the Chl^{surf} concentration estimate from satellite. However, as the satellite coverage is much greater than the *in situ* temperature/salinity coverage, this co-location procedure reduces the number of Chl^{surf} estimates available.

Second, defined as the "reanalysis dataset", we use a statistical reanalysis of ocean observation: the EN3 product produced by the UK Met-Office (http://www.metoffice.gov.uk/hadobs/en3/). The EN3 product consists of objective analyses formed from ship and Argo profile data. It provides monthly analysed fields of full-depth temperature and salinity profiles on a 1° grid. While the data are provided from 1950, we only used data from the year 2002 onward, when the objective analysis is constrained by Argo observations in the Southern Ocean. Although not independent (as EN3 assimilates Argo profiles), we compared mixed layer obtained from direct Argo profiles and from EN3 profiles. The comparison gives a correlation of 0.7, which gives us confidence that EN3 reanalysis is reasonable. We note that a careful evaluation of EN3 would involve re-running EN3 reanalysis, leaving some Argo profiles out, which is beyond the scope of this study.

MLD was extracted from individual profiles of the observational dataset and the reanalysis dataset. We calculated the MLD with a surface-density-difference criterion of $\Delta\sigma \leq 0.03\,\mathrm{kg\,m^{-3}}$ (de Boyer Montégut *et al.*, 2004; Sallée *et al.*, 2006). Sallée *et al.* (2006) tested a number of methods and show that this particular criterion is well adapted to find the base of the seasonal mixed layer in the Southern Ocean.

Where possible, we used the "observational dataset" to estimate MLD. However, when the analysis required the full length of the seasonal cycle (e.g. to reproduce the seasonal cycle of the mixed-layer integrated chlorophyll, or to compute the initiation date of the mixed-layer integrated chlorophyll), the "reanalysis dataset" was used.

For collocating the observational and reanalysis datasets to satellite-derived estimates of Chl^{surf}, we associated each Argo profiles or EN3 pixel to the closest (in space and time) pixel of ocean colour (so the largest distance in time is 4 d, and the largest distance in space is 6 km).

Water-column integrated chlorophyll

Although no observations of water-column integrated chlorophyll exist at large scales, in this study, we quantify this via the combination of surface satellite estimates of Chl^{surf} and interior ocean structure. We assume that chlorophyll is well mixed above the mixed-layer base, and that there is no chlorophyll below the mixed-layer base. Under such assumptions, we quantify the water-column integrated chlorophyll, Chl^{ML}, as:

$$Chl^{ML} = H \times Chl^{surf}, \quad (1)$$

where H is the MLD. We note that our assumptions may be questioned in spring when the MLD rapidly shallows, as under such conditions, some chlorophyll may be left below the mixed-layer base (e.g. Chiswell *et al.*, 2013; Franks, submitted to this issue). One therefore needs to be cautious of the interpretation of Chl^{ML} in spring.

We note that we assume here that Chl^{surf} and Chl^{ML} have the same seasonal pattern as, respectively, the surface biomass content and the mixed-layer integrated biomass content. In the Discussion section, we discuss the extent to this is true by attempting to compute the carbon concentration from Chl^{surf}, based on the chlorophyll-to-carbon ratio, Chl:C (Cloern *et al.*, 1995; Behrenfeld *et al.*, 2002): $Chl:C = Chl:C_{min} + [Chl:C_{max} - Chl:C_{min}]e^{-3Ig}$, where Ig is the mixed-layer integrated irradiance (in moles photons $m^{-2}\,h^{-1}$; calculation of Ig is described below, and is computed from NCEP Climate Forcing System Reanalysis outputs; see the Atmospheric fluxes section), $Chl:C_{min} = 0.004\,mgChl(mgC)^{-1}$, and $Chl:C_{max} = 0.013 mgChl(mgC)^{-1}$ (Behrenfield, 2010). We show that Chl^{surf} and C have very similar seasonal pattern.

Onset detection method

In this section, we describe the onset detection method that we apply to both Chl^{ML} and Chl^{surf} time-series. Hereafter, Chl^{ML}-onset will

refer to the date of onset detected on the Chl^{ML} time-series, and Chl^{surf}-onset to the date of onset detected on the Chl^{surf} time-series.

An important challenge is to identify the date of the start of intensification of chlorophyll (either Chl^{ML} or Chl^{surf}) in a manner that can be efficiently and accurately applied to a large datasets. Phenology studies currently use several methods to estimate the timing of a phytoplankton bloom. Ji *et al.* (2010) identify three broad categories of methods (see also Brody *et al.*, 2013): threshold method based on biomass; threshold method based on cumulative chlorophyll content; and rate of change methods. Threshold methods based on chlorophyll biomass define bloom initiation as the time at which a given threshold is reached (e.g. Siegel *et al.*, 2002; Vargas *et al.*, 2009; Thomalla *et al.*, 2011; Cole *et al.*, 2012; Sapiano *et al.*, 2012). Threshold methods based on cumulative chlorophyll biomass identify a bloom as the time at which a cumulative summation of chlorophyll biomass crosses a threshold percentile of the total biomass (e.g. Greve *et al.*, 2005; Mackas *et al.*, 2012). Finally, the rate of change methods estimate bloom initiation from the point of most rapid increase on a chlorophyll time-series or function fit to that time-series (e.g. Rolinski *et al.*, 2007; White *et al.*, 2009).

Brody *et al.* (2013) investigated the differences between these bloom detection methods. Their conclusion was that the first group of methods (chlorophyll biomass threshold) can be strongly biased for specific time-series and are well suited to investigating the match or mismatch between phytoplankton and upper trophic levels. The second group of methods (cumulative chlorophyll biomass threshold) is also very sensitive to the date used for the start of the time-series and thus cannot be implemented at the basin scale using a globally fixed start date (Brody *et al.*, 2013). Finally, the third group of methods (rate of change) identifies blooms when chlorophyll is increasing rapidly from the pre-bloom minimum, while absolute biomass levels may still remain low. These methods can be useful in examining the seasonal physical or biological mechanisms that create conditions in which a bloom can occur (Brody *et al.*, 2013).

Based on the analysis of Brody *et al.* (2013), we chose to apply a rate of change method that we designed and tuned for our dataset. At each grid-point of the chlorophyll dataset, a 13-year time-series (1998–2010) is extracted and linearly interpolated, and a fast Fourier transform low-pass filter is applied to remove any high-frequency (<3 months) variability irrelevant to seasonal time-scale and bloom onset. The bloom onset of one particular year is defined as the maximum of the second derivative of Chl (Chl_{tt}) in the time window where the derivative of Chl (Chl_t) (i) is positive, and (ii) contains a local maximum (here Chl is either Chl^{ML} or Chl^{surf}). If the bloom peak is below 1.2 times the seasonal minimum of Chl, we do not consider a bloom to have occurred. Our definition ensures that each defined onset is robust and exists as a bloom in the dataset. Additional constraints are applied to avoid unrealistic bloom detection: (i) the largest data-gap within the 4 months centred on the defined onset must be smaller than 45 d; (ii) the integrated amount of chlorophyll accumulated within 6 months before the onset must be <25% of the total amount of chlorophyll summed over the year, centred on the time of onset.

The Chl^{surf}-onset detection procedure nicely positions the Chl^{surf}-onset date at the start of the high Chl^{surf} season (Figure 2). We note however that in some instances, the detected Chl^{surf}-onset seems to be a bit late (e.g. Figure 2a in 2006; Figure 2a in 2010) compare with other cases where Chl^{surf}-onset appears detected in the very early days of the increasing season (e.g. Figure 2b in 2008). All automatic detection methods will have such caveats and errors associated with it (Cole *et al.*, 2012; Brody *et al.*, 2013). Cole *et al.* (2012) estimate the error on such automatic detection method to ~30 d in the Southern Ocean, which appears, by eyes, as a correct order of magnitude on the specific examples shown in Figure 2. We acknowledge that a definition "by eye" would produce in many instances a more robust definition of onset. However, our goal is to define an objective definition as robust as possible that can consistently treat more than 1 million seasonal cycles and investigate general basin-scale phenomena. We applied the same detection method on the Chl^{ML} time-series as an estimate of the bloom Chl^{ML}-onset date. Similar to the Chl^{surf}-onset date, we found the method reliable in detecting Chl^{ML}-onset as the starting date of the increased Chl^{ML} season (Figure 2).

Atmospheric fluxes

Atmospheric winds, buoyancy, and short-wave forcings are obtained from NCEP Climate Forcing System Reanalysis (http://cfs.ncep.noaa.gov/cfsr/). We used atmospheric fields from this reanalysis for the year 1998–2010, consistent with surface chlorophyll dataset time frame. The winds of the reanalysis product are strongly constrained by assimilation of satellite wind observation. However, we note that buoyancy flux fields remain poorly known in the Southern Ocean, and are only weakly constrained in atmospheric reanalysis efforts. These constraints are even weaker for freshwater fluxes. We therefore approximate the buoyancy flux to its heat component, which is less uncertain. Photosynthetically active radiation (PAR) relates to solar irradiance (I_r) following $PAR = 0.473 \times I_r$ (Papaioannou *et al.*, 1993). Mixed-layer integrated irradiance, Ig, is computed from downward short wave flux (in W m^{-2}):

$$Ig = \int_0^H I_0 e^{-kz} dz, \quad (2)$$

where I_0 is the downward short wave flux at sea surface, k the attenuation coefficient in the surface layer, and H the MLD. Attenuation coefficient depends on both water attenuation (k_w) and chlorophyll self-shading attenuation (k_{chl}). In this paper, we use $k_w = 0.02$ m^{-1} and k_{chl}=0.0865 m^{-1} (e.g. Nelson and Smith, 1991).

Results

Southern Ocean bloom Chl^{ML}-onset and Chl^{surf}-onset dates are estimated by a systematic method on more than 1 million seasonal cycles based on satellite-derived surface Chl^{surf} co-located with estimates of MLD (see the Material and methods section). Two time-series of Chl^{ML} and Chl^{surf}, and associated Chl^{ML}-onset and Chl^{surf}-onset dates are presented in Figure 2. These examples are chosen to represent two distinct regimes of blooms: one where Chl^{ML} is in phase with Chl^{surf} (Figure 2a), and one where Chl^{ML} and Chl^{surf} are slightly out of phase (Figure 2b).

The two time-series present a very marked seasonal cycle, with Chl^{surf} increasing by 3–5 times during the high activity season. The surface bloom clearly stands out as the period during which Chl^{surf} dramatically increases. Surface and mixed-layer integrated chlorophyll blooms have been described as tightly linked to the seasonal cycle of the MLD (e.g. Sverdrup, 1953; Behrenfeld, 2010). We therefore compare chlorophyll time-series with the collocated mixed-layer time-series (from the reanalysis dataset; see the Material and Methods section). The phasing between the

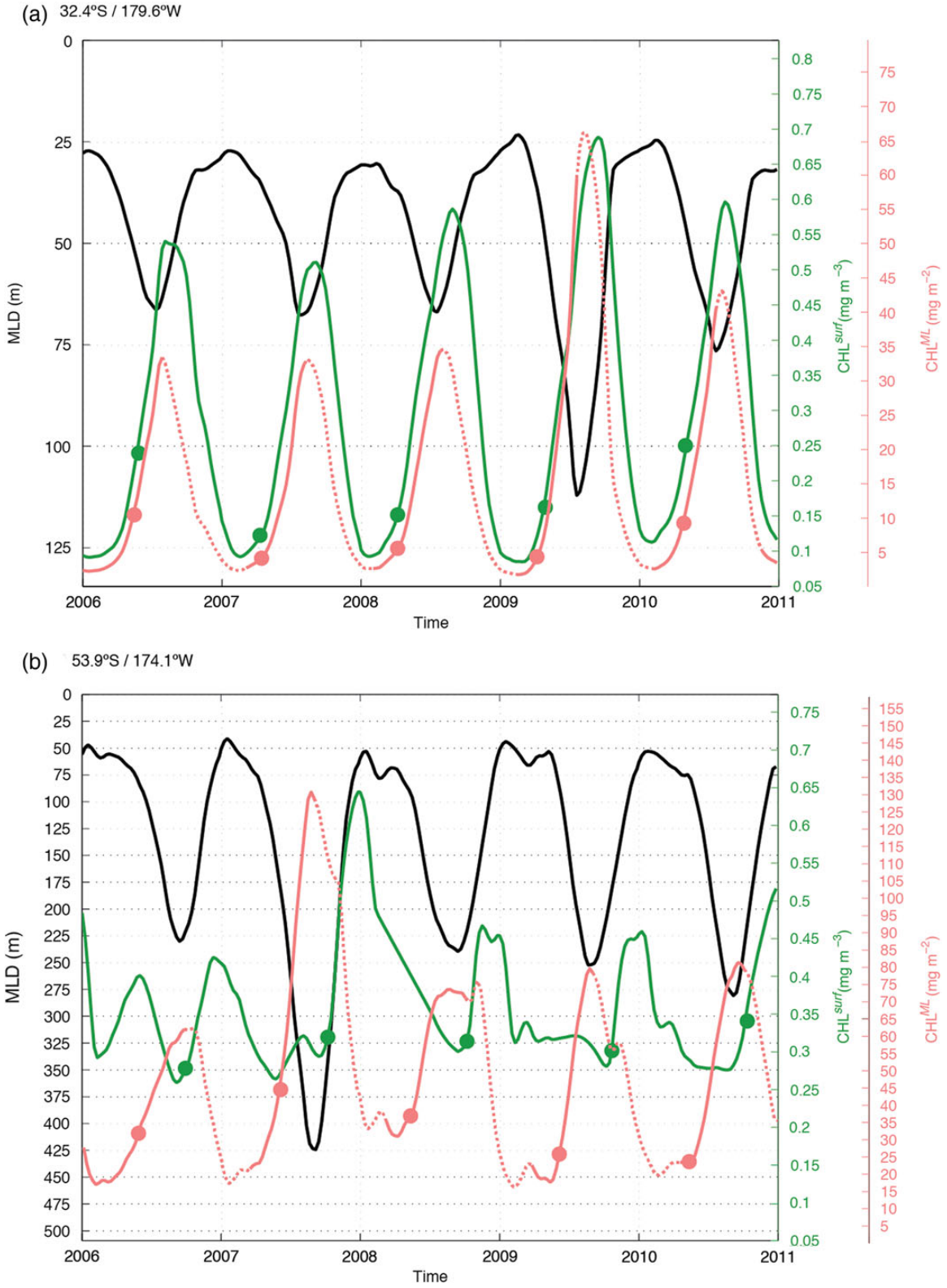

Figure 2. Two examples of time-series of (green) Chl_a in two distinct regions: (a) in a subtropical zone characterized by subtropical gyre circulation, at 32.4°S – 179.6°W; and (b) in a subantarctic zone, influence by the ACC dynamics, at 53.9°S – 174.1°W. Chl_a time-series is averaged over a region of 20 × 20 km centred on each location. For clarity, data are shown for 5 years, although the full time series are longer. Collocated (black) MLD and (pink) mixed-layer integrated chlorophyll time-series are superimposed on each panel. For each seasonal cycles at each locations, green dots indicate the Chl^{surf}-onset date and pink dots the Chl^{ML}-onset date detected by our automatic procedure (see text for details). Chl^{ML} is shown as dashed line during the mixed-layer restratification phase to remind the reader that our estimate of Chl^{ML} is questionable during this period (see text for details).

mixed-layer and the chlorophyll seasonal cycles appears consistent for different years of a given location, but clearly varies depending on the location (Figure 2). For instance, in Figure 2a, the surface chlorophyll bloom is associated with a deepening of the mixed layer, while in Figure 2b, the surface bloom is associated with a shallowing of the mixed layer. These two strikingly different regimes recall the debate around autumn vs. spring blooms (Lévy *et al.*, 2005; Chiswell *et al.*, 2013).

In the two example of Figure 2, we find that Chl^{ML}-onset and Chl^{surf}-onset can either be almost instantaneous or separated by a few months. We note that Chl^{ML}-onset is, here, always found during the deepening phase of the mixed layer, i.e. when the mixed layer actively convects, and where the assumption of a well-mixed chlorophyll profile in the mixed layer is the most robust. In the following, we undertake a systematic analysis of bloom Chl^{ML}-onset and Chl^{surf}-onset on the entire dataset to define specific bloom regimes, and next, we describe the seasonal cycles associated with each of the regimes.

Southern Ocean regimes of surface bloom

Over the entire database of Southern Ocean, the Chl^{ML}-onset dates organize around two main modes (Figure 3a). One mode, centred on May, is associated with autumn blooms that have a Chl^{ML}-onset before the winter solstice (21 June); the other mode, centred on July, is associated with winter blooms that have a Chl^{ML}-onset after the winter solstice. The winter solstice is a key date in the year as it corresponds to the date where incoming irradiance switches from declining to increasing (note, however, that one may argue that chlorophyll cares about the mixed-layer integrated irradiance, which can be distinct to incoming irradiance). The modal structure in Chl^{ML}-onset date could possibly be due to an unstable detection method picking very early Chl^{ML}-onsets in some instances and late Chl^{ML}-onsets in others (for instance, Figure 2 suggests that some Chl^{ML}-onsets are detected slightly later than what we would have picked by eye). To test the "stability" or "sensitivity" of the Chl^{ML}-onset detection procedure, we investigate the amount of accumulated chlorophyll at Chl^{ML}-onset. The percentage of accumulated chlorophyll at Chl^{ML}-onset is consistent over the entire database, with a clear and unique mode centred on 12.6% (Figure 3c). This result gives us confidence that the Chl^{ML}-onset detection procedure is stable enough to investigate bloom regimes in the Southern Ocean.

We then turn to the time-lag between Chl^{ML}-onset and Chl^{surf}-onset over the entire database. Two very clear modes stand out, with a group of blooms being characterized by almost parallel Chl^{ML}-onset and Chl^{surf}-onset, and a second group characterized by a lag of several months between Chl^{surf}-onset and Chl^{ML}-onset (Figure 3b).

Based on these Chl^{ML}-onset and Chl^{surf}-onset histograms, we define four Southern Ocean regimes: (regime 1) blooms with Chl^{ML}-onset before the winter solstice, and nearly parallel Chl^{surf}-onset (within 2 months); (regime 2a) blooms with Chl^{ML}-onset before the winter solstice, and with a significant lag between Chl^{ML}-onset and Chl^{surf}-onset (>2 months); (regime 2b) bloom with Chl^{ML}-onset after the winter solstice, and with a long time-lag between Chl^{ML}-onset and Chl^{surf}-onset (more than 2 months); and (regime 3) blooms with Chl^{ML}-onset after the winter solstice, and nearly parallel Chl^{surf}-onset (within 2 months). Ultimately, we seek to segregate blooms that occur before or after the winter solstice and blooms where integrated and surface biomass increase together or display a lag. For simplicity, in the remainder of this paper, we combine regime 2a and 2b, in a single "regime 2" since the regime 2a, and 2b did not show phenology different enough to be especially highlighted (not shown; regime 2 corresponds therefore to blooms with long time-lag between Chl^{ML}-onset and Chl^{surf}-onset). We remind the reader that we have, so far, made no assumption regarding geographic location, yet are able to group Southern Ocean chlorophyll blooms in three regimes. We now analyse the characteristics of each of these regimes.

We find that the three bloom regimes defined above display a coherent geographical organization (Figure 4). Blooms of regime 1 occur in a narrow zonal band between 30 and 40°S in the subtropics (except for the central Pacific basin, 80–160°W, that appears as an exception; Figure 4a) that are characterized by low surface nitrate concentrations (Figure 1d). Blooms of regime 2 are concentrated in the subantarctic region of the Southern Ocean: south of the subtropical front region and directly north of the Antarctic Circumpolar Fronts (Figure 4b). Finally, blooms of regime 3 are primarily associated with the fronts of the Antarctic Circumpolar (ACC; Figure 4c). Given the coherent geographical distribution associated with the three regimes, for convenience, we hereafter refer to them as "subtropical regime" for regime 1, "subantarctic regime" for regime 2, and "ACC regime" for regime 3. We note however that there are no clear geographical boundaries between the three regimes, which is consistent with the different blooms being driven by multiple processes (defined by a range of parameters, e.g. gyres, ACC, deep mixed-layers, iron inputs, etc.) rather than geographical bins.

The three regimes are associated with very distinct bloom characteristics. By definition, the subtropical regime has bloom Chl^{ML}-onsets centred in autumn (i.e. April–June; Figure 3a). Similarly, the ACC regime has bloom Chl^{ML}-onsets centred in winter (i.e. July–August; Figure 3a). Subantarctic regime Chl^{ML}-onset dates are mostly in autumn but some are in winter. All three regimes have their Chl^{ML}-onset during the period of convection, when air–sea heat fluxes are driving overturn of the surface layer (air–sea heat flux approximately -100 to -50 W m^{-2} at Chl^{ML}-onset; Figure 5a). In addition, the subantarctic and ACC regimes have their Chl^{ML}-onset when surface irradiance is low (short wave $\sim$50 W m^{-2} at Chl^{ML}-onset; Figure 5b), and daylight length is short ($\sim$9 h d^{-1}; Figure 5c).

Before investigating the details of the seasonal cycles, it is instructive to discuss the typical physical and biogeochemical conditions of the regions where each regime falls. Subtropical regimes are located in the centre of subtropical gyres, which are characterized by surface-depleted macronutrients and shallow winter mixed-layers (averaged MLD_{max} of 86 m and average surface nitrate concentration of 0.7 μmol kg^{-1}; Table 1 and Figure 1c and d). Therefore, we anticipate the availability of macronutrients will be the major regulator of blooms in these regions. In contrast, subantarctic and ACC regimes are located in the region of very deep winter mixed layers, much deeper than typical euphotic layers, and in regions richer in macronutrients (averaged MLD_{max} of 258 and 246 m, respectively, and average surface nitrate concentration of 11.8 and 11.9 μmol kg^{-1}; Table 1 and Figure 1c and d). Subantarctic and ACC regions are also known as HNLC regions. We therefore anticipate that these blooms will be governed by light and iron availability.

Seasonal cycles

For each of the three bloom regimes, we compute the median seasonal cycle of mixed layer, Chl^{ML} and Chl^{surf} (Figure 6). To

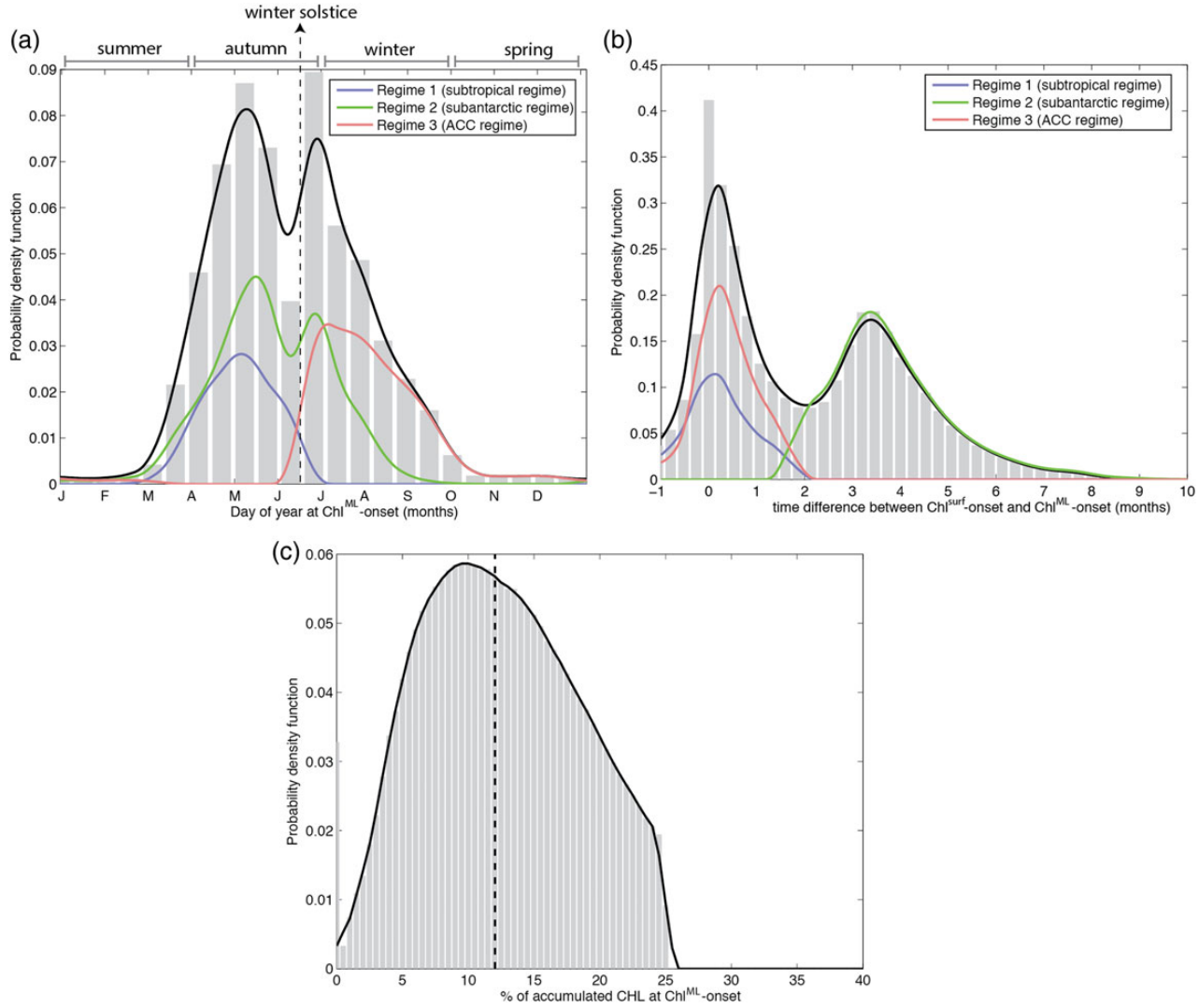

Figure 3. Probability density function (PDF) of the distribution of (a) the day of year of Chl^{ML}-onset; (b) the time difference between Chl^{ML}-onset and Chl^{surf}-onset; and (c) the percentage of accumulated chlorophyll at Chl^{ML}-onset. Grey bars show the PDF of the entire datasets. Smoothed PDF of (black) the entire dataset, and of (blue) regime 1, (green) regime 2, are (pink) regime 3 are superimposed on (a) and (b). Dashed line in (a) refers to the time of winter solstice. Dashed line in (c) denotes the median value of the distribution.

prevent the median from blurring Chl^{ML}-onset and the different phases of the bloom, we reference all seasonal cycles to their Chl^{ML}-onset date before averaging (see Supplementary material for more details). Similarly, we compute the mean seasonal cycle of air–sea heat flux, windstress, and downward short wave at ocean surface. We discuss the median seasonal cycle of each regime in turn, below.

The subtropical regime is marked by a Chl^{ML}-onset in autumn when the mixed layer deepens (Figure 6a). In this region, the Chl^{ML}-onset is parallel with the Chl^{surf}-onset. Chl^{ML}-onset occurs in a convective mixed layer (negative heat flux; Figure 6d) and when cycle of surface winds begins its seasonal increase. These characteristics rule out any control of Chl^{ML}-onset by a critical depth or critical stratification and points to control by the entrainment of macronutrients in the mixed layer associated with the deepening of the mixed layer. We note that the subtropical region is characterized by very low macronutrient concentrations in the surface layer (Table 1; Figure 1d), which supports the argument that the bloom herein is limited by the availability of nutrients. In addition, we note that the subtropical region is characterized by relatively shallow mixed layers (MLD_{max} of 85 ± 77 m; Table 1; Figure 1c), so light availability is likely to play a minor role in regulating blooms in this region. Although the Chl^{ML}-onset occurs at the seasonal minimum of mixed-layer integrated irradiance, the irradiance at this time is notably much larger than for subantarctic and ACC regimes (yellow lines in Figure 6d–f). The bloom in the subtropical regime continues for the entire mixed-layer deepening period, and weakens when the mixed layer reaches its maximum depth. Overall, the bloom seen at surface remains in phase with the integrated bloom over the year.

In contrast to the subtropical regime, the subantarctic regime is not in regions of low surface nitrate (Table 1; Figure 1d). The subantarctic regime Chl^{ML}-onset occurs in autumn, when the mixed layer starts destratifying (Figure 6b). Interestingly, the autumn–winter increase in Chl^{ML} is not seen at surface (i.e. on Chl^{surf}), which suggests that the actual increase in chlorophyll biomass is

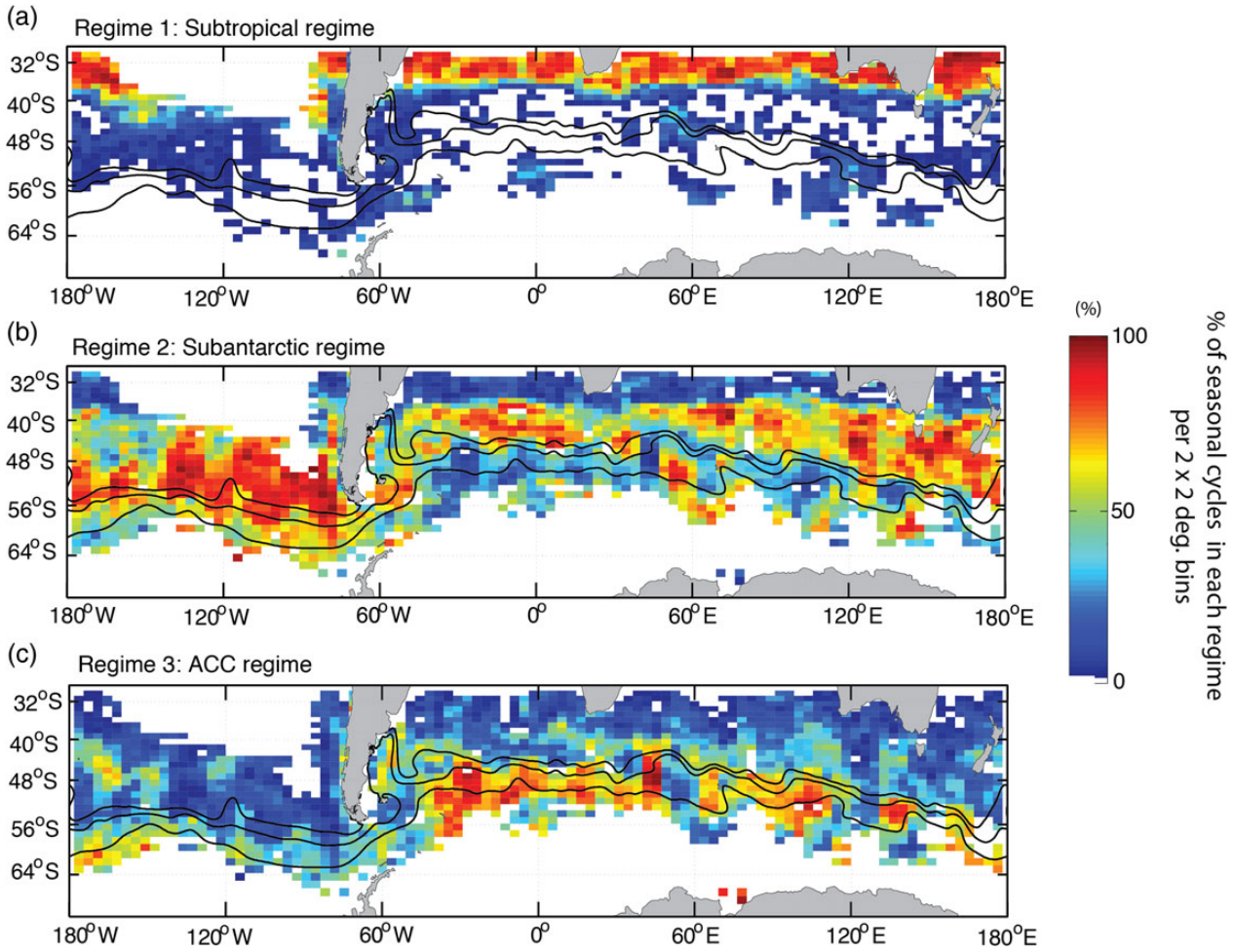

Figure 4. Geographical distribution of each bloom regime (see text for regime definition). The percentage of seasonal cycles associated with any given regime is gridded in 2 × 2°: (a) regime 1: subtropical blooms; (b) regime 2: subantarctic bloom; (c) regime 3: ACC blooms. In (a–c), the three black lines represent the approximate climatological position of the three main ACC branches, from south to north: Polar Front, subantarctic front, and northern branch of the subantarctic front following Sallée *et al.* (2008).

diluted in the increasing volume of the surface layer associated with mixed-layer deepening. Chl^{ML}-onsets in the subantarctic regime occur at low irradiance and in convective mixed layers (Figure 6e and f). When the mixed layer reaches its maximum depth in winter, the increase in Chl^{ML} stops (see in August in Figure 6b), and a second increase phase starts in early spring (star in Figure 6b). This second phase of the bloom is associated with a large surface signal (i.e. on Chl^{surf}) and is associated with Chl^{surf}-onset. It occurs during the restratification phase of the mixed layer (Figure 6b) and when light conditions rapidly increase (Figure 6e). The spring increase in Chl^{ML} in the subantarctic regime is therefore consistent with a light control of the bloom. However, this spring increase in Chl^{ML}, possibly light controlled, can begin in very deep mixed layers (up to 400–600 m, Figure 7a), which should rule out control by critical depth. Interestingly, we find that subantarctic Chl^{surf}-onsets are associated with air–sea heat fluxes switching from surface cooling to surface warming (Figures 6e and 7b).

Similar to the two other regimes, the ACC regime Chl^{ML}-onset occurs during the destratification phase of the mixed layer (Figure 6c). However, ACC regime blooms have their Chl^{ML}-onset in winter, later in the year compared with the other regimes. We note however that Chl^{ML}-onset of the ACC regime might be biased too late in the year, due to a weak bloom initiation. As such, one might say that Chl^{ML}-onset of ACC regime actually occurs in autumn (as the other regimes). However, the important point we wish to highlight is that the increase in integrated chlorophyll in autumn/winter in the ACC regime is, if anything, very low (Figure 6b and c). Chl^{surf} even decreases during autumn months (Figure 6b), suggesting that the autumnal growth is so low that it cannot compensate for the dilution associated with the deepening of the mixed-layer base. Then, in winter, when the MLD reaches its seasonal maximum, a very large and sudden increase in Chl^{ML} starts. In contrast to the subantarctic regime, the autumn–winter increase in Chl^{ML} happens at the end of the MLD deepening season, so the increase in integrated chlorophyll is not diluted in increasing volume of the surface layer. The chlorophyll increase signal translates therefore very clearly on Chl^{surf} (Figure 6b). This winter increase in Chl^{ML} and Chl^{surf} starts at low irradiance, in convective mixed layers (Figures 6f and 7b) and in deep mixed layers (up to 200–300 m; Figure 7a). The bloom continues over in spring when mixed layer restratifies and light condition improves.

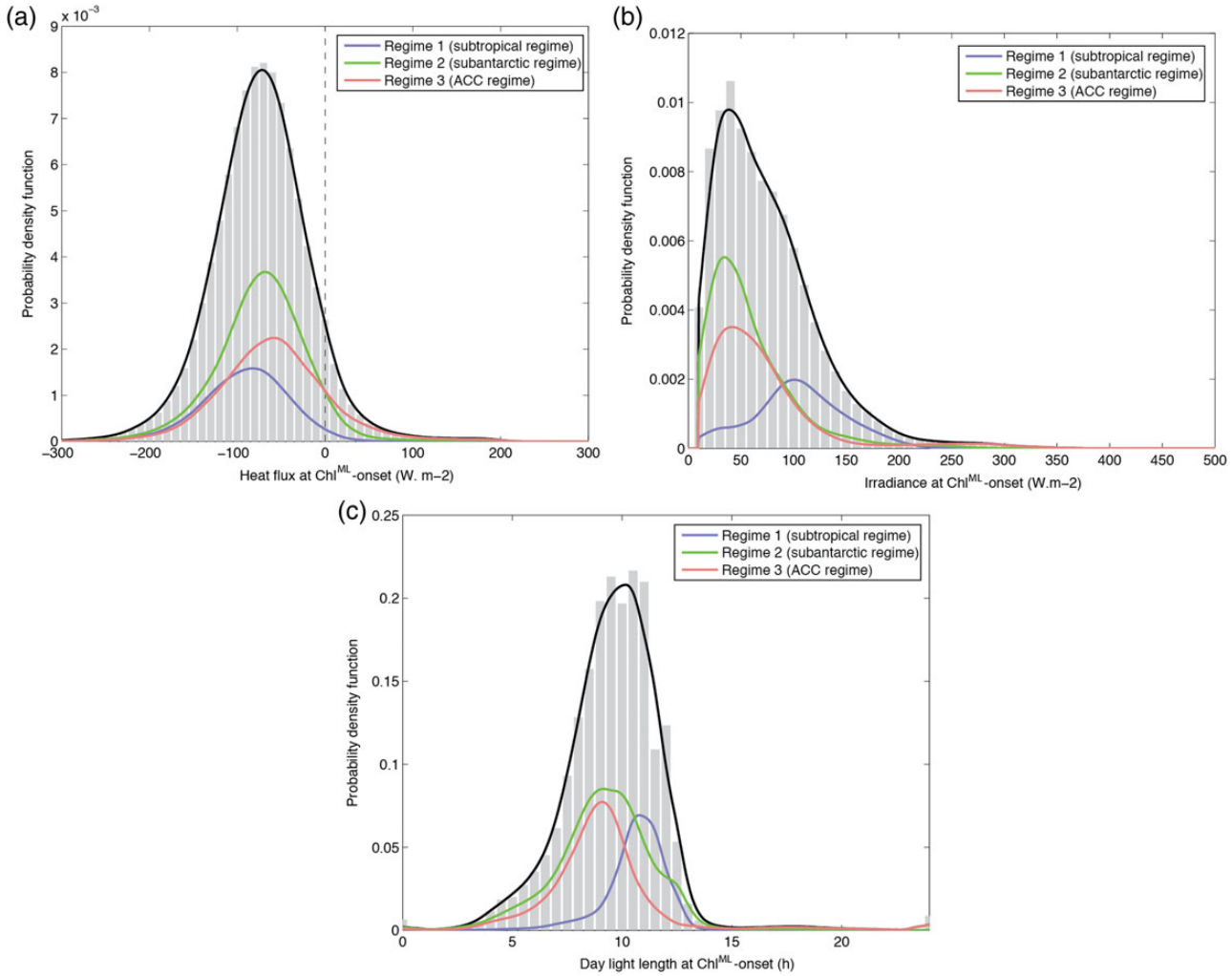

Figure 5. Probability density function (PDF) of the distribution of (a) daylight length at the time of Chl^{ML}-onset (h); (b) surface irradiance at Chl^{ML}-onset (W m^{-2}); and (c) the intensity of air–sea heat flux at Chl^{ML}-onset (negative denotes an ocean cooling; W m^{-2}). Grey bars show the PDF of the entire datasets. Smoothed PDF of (black) the entire dataset, and of (blue) regime 1, (green) regime 2, are (pink) regime 3 are superimposed.

Table 1. Climatological mean biogeochemical and physical surface characteristics values in each of the three regimes.

	Subtropical regime	Subantarctic regime	ACC regime
MLD_{max} (m)	85.77 ± 27.71	257.80 ± 104.86	245.62 ± 105.67
Nitrate (μmol kg^{-1})	0.71 ± 0.77	11.79 ± 6.44	11.91 ± 7.22

MLD_{max} refers to the climatological winter depth of mixed layer (from Argo; Sallée *et al.*, 2010). Nitrate are climatological mean surface values from World Ocean Atlas. Averages are weighted by the geographical distribution of the number of profiles for each regime.

Discussion

Overall, we find that all three regimes found in the present study have their Chl^{ML}-onset in autumn–winter when the solar irradiance is at its seasonal minimum, when daylight length is short, and when mixed layer actively mixes. While the phenological differences between the three regimes clearly standout in our observational dataset, linking these differences to biological and physical control is challenging from the available observations. The year-round biogeochemical water-column observations necessary to determine the factors that control the different phases of the bloom are currently not available. Nevertheless, we can speculate on the distinct controlling factors of each regime.

The subtropical regime is specific since it is located in a region of much stronger nitrate limitation (Table 1; Figure 1d) and relatively higher year-round light levels than the wider Southern Ocean. We find that the Chl^{ML}-onset in the subtropical regime occurs as soon as the mixed layer deepens in fall and entrains subsurface nitrate. The bloom then reaches its apex (i.e. date of maximum Chl^{ML}) when the MLD is maximal. While we cannot disentangle the potential roles of dilution and nutrients with our dataset, the strong degree of nitrate limitation in this region implies this is most likely to be a bloom controlled by nitrate entrainment. In that sense, the subtropical regime bloom Chl^{ML}-onsets can be considered to be in a bottom-up regime.

In the subantarctic regime, the deepening of the mixed-layer in autumn–winter dilutes the surface layer, which will reduce the prey-grazer encounter rate. However, for a bloom to be efficiently initiated by the reduction in the prey-grazer encounter rate, the

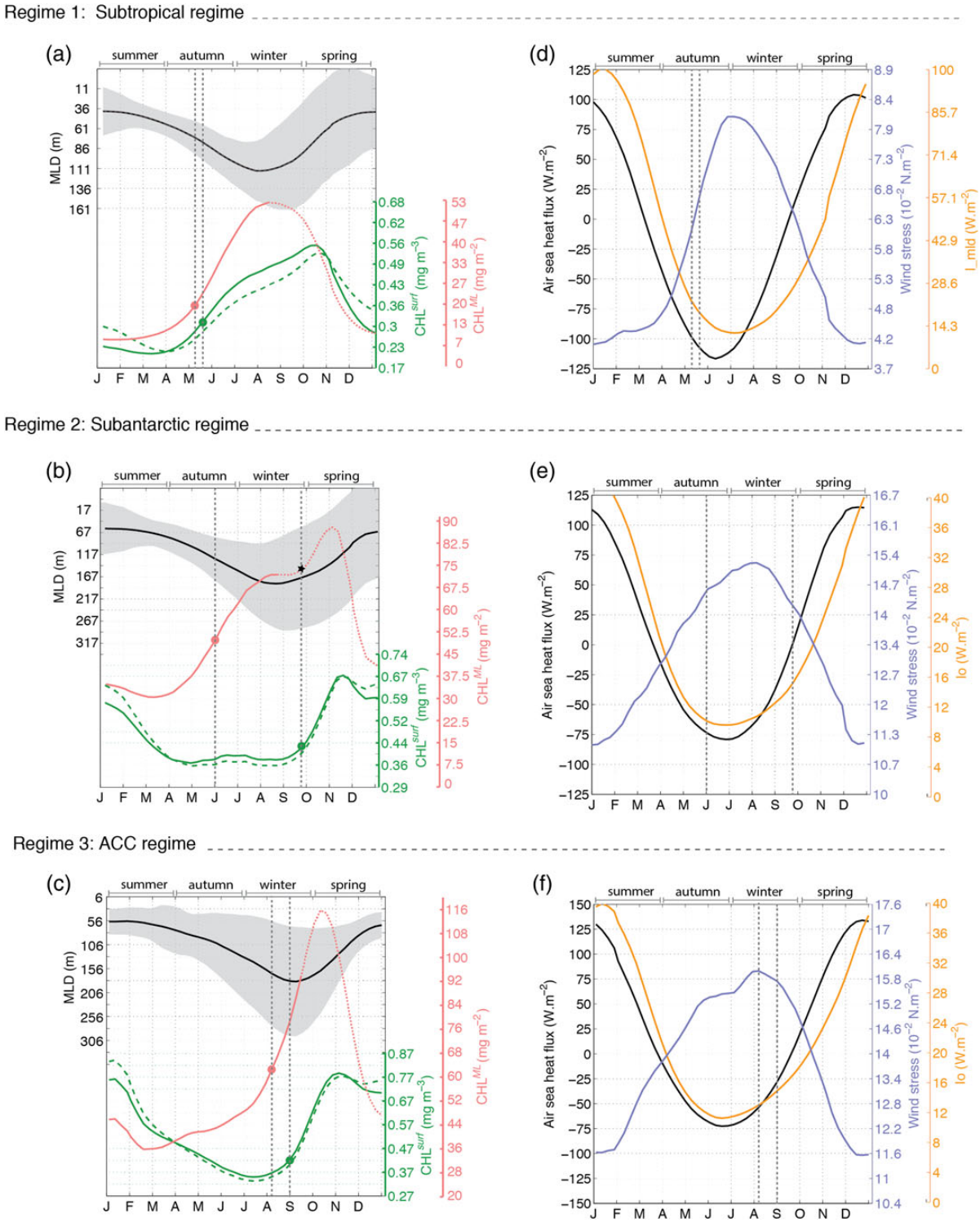

Figure 6. Median of all seasonal cycles falling in (a and d) subtropical regime; (b and e) subantarctic regime; (c and f) ACC regime. Before taking the mean, all seasonal cycles are centred on their date of Chl^{ML}-onset. (a – c) show the seasonal cycles of: (plain green) surface Chl_a (mg m^{-3}); (dashed green) associated surface carbon biomass (mg C); (pink) mixed-layer integrated chlorophyll, Chl^{ML} (mg m^{-2}); (black) MLD from collocated *in situ* observation (m). Surface carbon biomass reads on the surface Chl_a axis, and has been multiplied by the following values to scale with Chl_a: (a) 0.0124; (b) 0.0122; (c) 0.0098. (d – f) show the seasonal cycles of: (black) air – sea heat flux (W m^{-2}); (purple) windstress (N m^{-2}); and (yellow) mixed-layer averaged irradiance (W m^{-2}). In (a-c), green dots indicate the median Chl^{surf}-onset date and pink dots the median Chl^{ML}-onset date detected by our automatic procedure (see text for details). Chl^{ML} is shown as a dotted line during the mixed-layer restratification phase because our estimate of Chl^{ML} is questionable during this period (see text for details). In (b), the black star on the Chl^{ML} curves denotes the time of Chl^{surf}-onset. Chl^{surf} -onset and Chl^{ML}-onset are reported on all panels by the vertical grey dashed lines. In (a – c), grey shadings denote the 1 s.d. envelop around the median value.

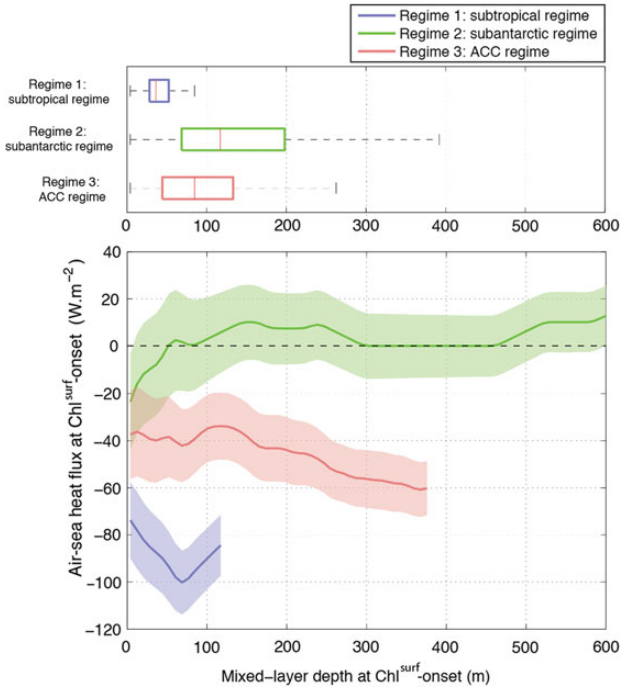

Figure 7. (a) Box plot of the mixed layer depth at Chl^{surf}-onset for each regime. (b) Air–sea heat flux at Chl^{surf}-onset vs. MLD at Chl^{surf}-onset: (plain curve) mean and (shading) standard deviation are shown for each regime. In both panels, the colour refers to bloom regime: (blue) subtropical regime; (green) subantarctic regime; and (pink) ACC regime.

system must at least be supporting some low levels of growth, or the growth must decline slower than the reduction in loss associated with the diminished prey-grazer encounter rate (e.g. Llort *et al.*, this issue). Again, this is difficult to assess, but we do observe a significant autumnal accumulation of integrated chlorophyll, which suggests some growth is occurring at the time of mixed layer deepening, or that losses are reducing faster than growth. In addition, Chl^{surf} remains constant in autumn (Figure 6b), while we know that the mixed layer is deepening at this seasons, which is an evidence that some growth must occur to balance the increase in the surface-layer volume. Therefore, perhaps dilution, lowering prey-grazer encounter rate, may stimulate this bloom and that the autumn–winter subantarctic regime bloom Chl^{ML}-onsets are a top-down controlled regime.

The subantarctic regime is also noteworthy in that in contains a spring increase in Chl^{ML} after the autumn–winter increase. This spring increase translates into a large surface signal, and is therefore associated with Chl^{surf}-onset. Interestingly, this spring increase in Chl^{ML} can start in either deep or shallow mixed layers (Figure 7a). However, for mixed layer deeper than 50 m or so, it consistently starts when air–sea heat fluxes switch from cooling the surface layer to warming (Figure 7b). Taylor and Ferrari (2011a, b) proposed that the date at which air–sea heat flux switches from cooling to warming would be a good proxy for the date at which turbulence in the mixed layer would drop. Indeed, as mixed-layer turbulence ceases the degree of light limitation reduces (e.g. Huisman *et al.*, 1999). This improvement of the light environment associated with a more stable mixed layer can explain spring Chl^{ML} increase in this region. When mixed layers are very shallow (below 50 m or so), light is not limiting, and spring increase starts earlier (in negative air–sea heat fluxes).

In the ACC regime, the autumn–winter dilution is not able to initiate the bloom. Instead, there is very little chlorophyll accumulation in autumn, suggestive of chronic limitation of growth and ruling out a strong role for dilution (Llort *et al.*, this issue). A large integrated chlorophyll accumulation only starts when the mixed layer reaches its winter maximum. In the absence of dilution, a plausible explanation is that strong iron limitation in the ACC regime prevents the autumnal dilution from triggering the bloom. It is only when the mixed layers reach deep iron reservoir in winter that iron limitation is alleviated (e.g. Tagliabue *et al.*, 2014). In parallel, light conditions start to improve and we therefore speculate that the combination of light and iron initiates a short and intense bottom-up controlled bloom in the ACC regime.

An implication of our interpretation is that the subantarctic regime is assumed to be less iron-limited than the ACC regime, which allows for some autumnal growth (permitting therefore the top-down controlled autumn–winter bloom) and permits the spring secondary bloom not seen in the ACC. This may manifest itself due to differences between the two regions in total iron inputs or in iron recycling (Boyd *et al.*, 2012; Tagliabue *et al.*, 2014). At present, we do not have enough observations of dissolved iron, particularly at the times of seasonal transitions (Tagliabue *et al.*, 2012), nor do we have a broad enough understanding of the seasonal patterns of iron limitation (e.g. Moore *et al.*, 2013; Tagliabue *et al.*, 2014) to address this at basin scale and over the full length of seasonal cycle. However, it is notable that the subantarctic regime contains the largest number of continental sources of iron in the Southern Ocean (e.g. South America, Falkland Islands, South Africa, Crozet Island, Tasmania, New Zealand; the only notable exception being Kerguelen Island). This consistently translates into the presence of large blooms and maximum iron utilization in the subantarctic region, downstream of the major western boundary currents flowing on the northern edge of the ACC, as estimated from satellite imagery (Figure 1a; e.g. Sokolov and Rintoul, 2007; Thomalla *et al.*, 2011; Boyd *et al.*, 2012).

Llort *et al.* (this issue) found that onset identified from Chl^{ML} corresponded in more than 85% of cases to the bloom onset detected from the actual water-column integrated biomass of their model (see also Sverdrup, 1953; Behrenfeld *et al.*, 2010). In addition, they found that Chl^{surf}-onset is associated with the climax of the bloom, which corresponds to the date of maximum integrated chlorophyll increase. Chl^{ML}-onset and Chl^{surf}-onset, which we use to describe bloom regimes, are therefore associated with two distinct key dates of bloom phenology. As noted by Llort *et al.* (this issue), some confusion in our understanding of chlorophyll bloom might have arisen from the use of the same word "onset" to 'refer to either Chl^{ML}-onset (e.g. Sverdrup, 1953; Behrenfeld *et al.*, 2010) or Chl^{surf}-onset (e.g. Lozier *et al.*, 2011; Ferrari *et al.*, 2014). Indeed, our results clearly indicate that Chl^{ML}-onset and Chl^{surf}-onset refer to different phases of the bloom with arguably distinct controlling factors (see also Llort *et al.*, this issue).

One potential caveat in studying chlorophyll blooms from surface estimate of Chl^{surf} is that an increase in Chl^{surf} can be produced by photoadaptation rather than an increase in biomass. To test this, we computed the carbon concentration from Chl^{surf} based on the chlorophyll-to-carbon ratio, Chl:C (e.g. Cloern *et al.*, 1995; Behrenfeld *et al.*, 2002; see the Material and methods section). We find that in all three regimes, the increase in surface

chlorophyll does coincide with the increase in carbon biomass (Figure 6a–c). Another important assumption in our study is that chlorophyll is well mixed in the mixed layer. We note that the three regimes described in this paper do not rely only on Chl^{ML}, but are also clearly identified as three distinct patterns on surface chlorophyll (Figure 6a–c). In addition, Chl^{ML}-onsets are detected in the deepening phase of the mixed layer, when active convection occurs and where we are confident that phytoplankton are actively mixed over the MLD. Subsurface chlorophyll directly beneath the base of the surface layer when the mixed layer is shallow in summer has been observed in the ocean (e.g. Holm-Hansen and Hewes, 2004), which would question our assumption regarding the vertical structure of chlorophyll, and could cause an increase in surface chlorophyll without increase in biomass through resuspension of a subsurface chlorophyll maximum. Although the presence of such subsurface chlorophyll would affect our results, we note that summer mixed layer in the subantarctic and ACC regions are of order of 50–100 m (e.g. Sallée *et al.*, 2010), so we are confident that light limitation in these regions would prevent chlorophyll to be maintain year-round under the base the mixed layer. Making these assumptions has allowed us to identify three main bloom regimes of the Southern Ocean, as well as their distinct phenologies (autumn, winter, and spring blooms). Future work will however need to be dedicated to the study of these regimes from *in situ* datasets. The growing bio-argo programme that reports concomitant biological and physical observations, year-round, will no doubt be of great help in assessing the details of the three main regimes identified in this paper.

Conclusion

The bloom Chl^{ML}-onset and Chl^{surf}-onset in the Southern Ocean have been estimated from satellite-derived products and observation-based estimates of MLD. Our automatic procedure was applied systematically over a large dataset, which allows us to illustrate basin scale regimes of bloom dynamics. The phenology of phytoplankton blooms appears organized into three distinct regimes when analysing Chl^{ML}-onset and Chl^{surf}-onset dates. These regimes are associated with three specific geographic locations: (i) autumn Chl^{ML}-onset (i.e. before winter solstice) blooms in a single phase (i.e. almost parallel Chl^{surf}-onset and Chl^{ML}-onset) are found in the subtropics, (ii) autumn–winter blooms with a second increase in spring (i.e. Chl^{surf}-onset and Chl^{ML}-onset separated by a few months) are found in the subantarctic zone (between the ACC and the subtropics), and (iii) winter Chl^{ML}-onset (i.e. after winter solstice) blooms in a single phase (i.e. almost parallel Chl^{surf}-onset and Chl^{ML}-onset) are found in the ACC region. It is notable that these three regimes organize themselves coherently in geographical space that is mostly zonal (except the central Pacific basin, 80–160°W, that appears as an exception for the subtropical regime, with almost no bloom in the region; Figure 4). However, the subantarctic and ACC regimes clearly follow the known meridional deviations and standing meanders of the ACC. Our findings suggest that the three regimes are fundamentally controlled by distinct mixed-layer and nutrient characteristics.

In summary, we find that autumn–winter blooms in the subtropical and ACC regimes are bottom-up controlled, associated with entrainment of nutrient (nitrate for the subtropical regime, and iron for the ACC regime). The autumn bloom in the subantarctic regime is top-down controlled, associated with a reduction in prey-grazer encounter when the mixed-layer destratifies. This subantarctic regime autumn bloom is followed by a bottom-up controlled spring bloom, associated with rapid light improvement in the surface layer, which is caused by a reduction in surface-layer turbulence.

Supplementary data

Supplementary material is available at *ICESJMS* online version of the manuscript.

Acknowledgements

We thank two anonymous reviewers and R. Johnson for their comments and suggestions that improved the manuscript. We thank R. Johnson for kindly providing his reprocessed ocean colour dataset, specifically treated for the Southern Ocean. R. Johnson originally used satellite data provided by NASA Goddard Space Flight Centre and the ESA GlobColour Project. We also thank J. Le Sommer and L. Bopp for the interesting discussions that partly motivated this work. The Argo float data were collected and made freely available by the International Argo Program (http://www.argo.ucsd.edu). J-BS received support from Agence Nationale de la Recherche (ANR), ANR-12-PDOC-0001, as well as from the British Antarctic Survey as a BAS Fellow.

References

Arrigo, K. R., van Dijken, G. L., and Bushinsky, S. 2008. Primary production in the Southern Ocean, 1997–2006. Journal of Geophysical Research, 113: C08004.

Behrenfeld, M. J. 2010. Abandoning Sverdrup's critical depth hypothesis on phytoplankton blooms. Ecology, 91: 977–989.

Behrenfeld, M. J., Marañón, E., Siegel, D. A., and Hooker, S. B. 2002. Photoacclimation and nutrient-based model of light-saturated photosynthesis for quantifying oceanic primary production. Marine Ecology Progress Series, 228: 103–117.

Boss, E., and Behrenfeld, M. 2010. In situ evaluation of the initiation of the North Atlantic phytoplankton bloom. Geophysical Research Letters, 37: L18603.

Boyd, P. W. 2002. The role of iron in the biogeochemistry of the Southern Ocean and equatorial Pacific: a comparison of in situ iron enrichments. Deep Sea Research II: Topical Studies in Oceanography, 49: 1803–1821.

Boyd, P. W., Arrigo, K. R., Strzepek, R., and van Dijken, G. L. 2012. Mapping phytoplankton iron utilization: insights into Southern Ocean supply mechanisms. Journal of Geophysical Research, 117: C06009.

Boyd, P. W., and Ellwood, M. J. 2010. The biogeochemical cycle of iron in the ocean. Nature Geoscience, 3: 675–682.

Brody, S. R., Lozier, M. S., and Dunne, J. P. 2013. A comparison of methods to determine phytoplankton bloom initiation. Journal of Geophysical Research: Oceans, 118: 2345–2357.

Carranza, M., and Gille, S. T. 2015. Southern Ocean wind-driven entrainment enhances satellite chlorophyll-a through the summer. Journal of Geophysical Research: Oceans, 120: 304–323.

Chiswell, S. M., Bradford-Grieve, J., Hadfield, M. G., and Kennan, S. C. 2013. Climatology of surface chlorophyll a, autumn–winter and spring blooms in the southwest Pacific Ocean. Journal of Geophysical Research: Oceans, 118: 1003–1018.

Cloern, E. J., Grenz, C., and Vidergar-Lucas, L. 1995. An empirical model of the phytoplankton chlorophyll:carbon ratio—the conversion factor between productivity and growth rate. Limnology and Oceanography, 40: 1313–1321.

Cole, H., Henson, S., Martin, A., and Yool, A. 2012. Mind the gap: the impact of missing data on the calculation of phytoplankton phenology metrics. Journal of Geophysical Research, 117: C08030.

de Boyer Montégut, C., Madec, G., Fischer, A. S., Lazar, A., and Iudicone, D. 2004. Mixed layer depth over the global ocean: an examination of profile data and a profile-based climatology. Journal of Geophysical Research, 109: C12003.

Evans, G. T., and Parslow, J. S. 1985. A model of annual plankton cycles. Biological Oceanography, 3: 327–347.

Ferrari, R., Merrifield, S., and Taylor, J. 2014. Shutdown of convection triggers increase of surface chlorophyll. Journal of Marine Systems, 1–32. doi:10.1016/j.jmarsys.2014.02.009.

Franks, P. J. S. Has Sverdrup's critical depth hypothesis been tested? Mixed layers vs. turbulent layers. ICES Journal of Marine Science, doi: 10.1093/icesjms/fsu175.

Frants, M., Gille, S. T., Hatta, M., Hiscock, W. T., Kahru, M., Measures, C. I., Mitchell, B. G., *et al.* 2013. Analysis of horizontal and vertical processes contributing to natural iron supply in the mixed layer in southern Drake Passage. Deep Sea Research II: Topical Studies in Oceanography, 90: 68–76.

Gran, H. H., and Braarud, T. 1935. A quantitative study of the phytoplankton in the Bay of Fundy and the Gulf of Maine (including observations on hydrography, chemistry and turbidity). Journal of the Biological Board of Canada, 1: 279–467.

Greve, W., Prinage, S., Zidowitz, H., Nast, J., and Reiners, F. 2005. On the phenology of North Sea ichthyoplankton. ICES Journal of Marine Science, 62: 1216–1223.

Henson, S., Cole, H., Beaulieu, C., and Yool, A. 2013. The impact of global warming on seasonality of ocean primary production. Biogeosciences, 10: 4357–4369.

Holm-Hansen, O., and Hewes, C. D. 2004. Deep chlorophyll-a maxima (DCMs) in Antarctic waters. Polar Biology, 27: 699–710.

Huisman, J., van Oostveen, P., and Weissing, F. J. 1999. Critical depth and critical turbulence: two different mechanisms for the development of phytoplankton blooms. Limnology and Oceanography, 44: 1781–1787.

Ji, R., Edwards, M., Mackas, D. L., Runge, J. A., and Thomas, A. C. 2010. Marine plankton phenology and life history in a changing climate: current research and future directions. Journal of Plankton Research, 32: 1355–1368.

Johnson, R., Strutton, P. G., Wright, S. W., McMinn, A., and Meiners, K. M. 2013. Three improved satellite chlorophyll algorithms for the Southern Ocean. Journal of Geophysical Research: Oceans, 118: 3694–3703.

Lévy, M., Lehahn, Y., Andre, J-M., Mémery, L., Loisel, H., and Heifetz, E. 2005. Production regimes in the northeast Atlantic: a study based on Sea-viewing Wide Field-of-view Sensor (SeaWiFS) chlorophyll and ocean general circulation model mixed layer depth. Journal of Geophysical Research, 110: C07S10.

Llort, J., Lévy, M., Sallée, J. B., and Tagliabue, A. 2015. Onset, intensification and decline of phytoplankton blooms in the Southern Ocean. ICES Journal of Marine Science, this issue.

Longhurst, A., Sathyendranath, S., Platt, T., and Caverhill, C. 1995. An estimate of global primary production in the ocean from satellite radiometer data. Journal of Plankton Research, 17: 1245–1271.

Lozier, S., Dave, A. C., Palter, J., Gerber, L. M., and Barber, R. T. 2011. On the relationship between stratification and primary productivity in the North Atlantic. Geophysical Research Letters, 38: L18609.

Mackas, D. L., Greve, W., Edwards, M., Chiba, S., Tadokoro, K., Eloire, D., Mazzocchi, M. G., *et al.* 2012. Changing zooplankton seasonality in a changing ocean: comparing time series of zooplankton phenology. Progress in Oceanography, 97–100: 31–62.

Mahadevan, A., Dasaro, E., Lee, C., and Perry, M. J. 2012. Eddy-driven stratification initiates North Atlantic spring phytoplankton blooms. Science, 337: 54–58.

Martin, J. H., Fitzwater, S. E., and Gordon, R. M. 1990. Iron deficiency limits phytoplankton growth in Antarctic waters. Global Biogeochemical Cycles, 4: 5–12.

Moore, C. M., Mills, M. M., Arrigo, K. R., Berman-Frank, I., Bopp, L., Boyd, P. W., Galbraith, E. D., *et al.* 2013. Processes and patterns of oceanic nutrient limitation. Nature Geoscience, 6: 701–710.

Moore, J. K., and Abbott, M. R. 2002. Surface chlorophyll concentrations in relation to the Antarctic Polar Front: seasonal and spatial patterns from satellite observations. Journal of Marine Systems, 37: 69–86.

Nelson, D. M., and Smith, W. O. 1991. Sverdrup revisited: critical depths, maximum chlorophyll levels, and the control of Southern Ocean productivity by the irradiance-mixing regime. Limnology and Oceanography, 36: 1650–1661.

Papaioannou, G., Papanikolaou, N., and Retalis, D. 1993. Relationships of photosynthetically active radiation and shortwave irradiance. Theoretical and Applied Climatology, 48: 23–27.

Riley, G. A. 1946. Factors controlling phytoplankton populations on Georges Bank. Journal of Marine Research, 6: 54–73.

Rintoul, S. R., Hughes, C. W., and Olbers, D. 2001. The Antarctic circumpolar current system. *In* Ocean Circulation and Climate, pp. 271–302. Ed. G. Siedler, J. Church, and J. Gould. Academic Press, New York.

Rolinski, S., Horn, H., Petzoldt, T., and Paul, L. 2007. Identifying cardinal dates in phytoplankton time series to enable the analysis of long-term trends. Oecologia, 153: 997–1008.

Ryther, J. H., and Hulburt, E. M. 1960. On winter mixing and the vertical distribution of phytoplankton. Limnology and Oceanography, 5: 337–338.

Sallée, J. B., Speer, K., and Morrow, R. 2008. Response of the Antarctic Circumpolar Current to atmospheric variability. Journal of Climate, 21: 3020–3039.

Sallée, J. B., Speer, K., Rintoul, S., and Wijffels, S. 2010. Southern Ocean thermocline ventilation. Journal of Physical Oceanography, 40: 509–529.

Sallée, J. B., Wienders, N., Speer, K., and Morrow, R. 2006. Formation of subantarctic mode water in the southeastern Indian Ocean. Ocean Dynamics, 56: 525–542.

Sapiano, M. R. P., Brown, C. W., Schollaert Uz, S., and Vargas, M. 2012. Establishing a global climatology of marine phytoplankton phenological characteristics. Journal of Geophysical Research, 117: C08026.

Sarmiento, J. L., Gruber, N., Brzezinski, M. A., and Dunne, J. P. 2004. High-latitude controls of thermocline nutrients and low latitude biological productivity. Nature, 427: 56–60.

Siegel, D. A., Doney, S. C., and Yoder, J. A. 2002. The North Atlantic spring phytoplankton bloom and Sverdrup's critical depth hypothesis. Science, 296: 730.

Sokolov, S., and Rintoul, S. R. 2007. On the relationship between fronts of the Antarctic Circumpolar Current and surface chlorophyll concentrations in the Southern Ocean. Journal of Geophysical Research, 112: C07030.

Sverdrup, H. U. 1953. On conditions for the vernal blooming of phytoplankton. Journal du Conseil International pour l'Exploration de la Mer, 18: 287–295.

Tagliabue, A., Mtshali, T., Aumont, O., Bowie, A. R., Klunder, M. B., Roychoudhury, A. N., and Swart, S. 2012. A global compilation of dissolved iron measurements: focus on distributions and processes in the Southern Ocean. Biogeosciences, 9: 2333–2349.

Tagliabue, A., Sallée, J. B., Bowie, A. R., Lévy, M., Swart, S., and Boyd, P. W. 2014. Surface-water iron supplies in the Southern

Ocean sustained by deep winter mixing. Nature Geoscience, 7: 314–320.

Taylor, J. R., and Ferrari, R. 2011a. Ocean fronts trigger high latitude phytoplankton blooms. Geophysical Research Letters, 38: L23601.

Taylor, J. R., and Ferrari, R. 2011b. Shutdown of turbulent convection as a new criterion for the onset of spring phytoplankton blooms. Limnology and Oceanography, 56: 2293–2307.

Thomalla, S. J., Fauchereau, N., Swart, S., and Monteiro, P. M. S. 2011. Regional scale characteristics of the seasonal cycle of chlorophyll in the Southern Ocean. Biogeosciences, 8: 2849–2866.

Townsend, D. W., Kelle, M. D., Sieracki, M. E., and Ackleson, S. G. 1992. Spring phytoplankton blooms in the absence of vertical water column stratification. Nature, 360: 59–62.

Vargas, M., Brown, C. W., and Sapiano, M. R. P. 2009. Phenology of marine phytoplankton from satellite ocean color measurements. Geophysical Research Letters, 36: L01608.

White, M. A., de Beurs, K. M., Didan, K., Inouye, D. W., Richardson, A. J., Jensen, O. P., O'Keefe, J., *et al.* 2009. Intercomparison, interpretation, and assessment of spring phenology in North America estimated from remote sensing for 1982–2006. Global Change Biology, 15: 2335–2359.

Handling editor: Rubao Ji